Memory CD8$^+$ T cells balance pro- and anti-inflammatory activity by reprogramming cellular acetate handling at sites of infection

Maria L. Balmer[1,10,11], Eric H. Ma[2], Andrew Thompson[3], Raja Epple[1], Gunhild Unterstab[1], Jonas Lötscher[1], Philippe Dehio[1], Christian M. Schürch[4], Jan D. Warncke[1], Gaëlle Perrin[1], Anne-Kathrin Woischnig[5], Jasmin Grählert[1], Jordan Löliger[1], Nadine Assmann[1], Glenn R. Bantug[1], Olivier P. Schären[6], Nina Khanna[5], Adrian Egli[7], Lukas Bubendorf[8], Katharina Rentsch[9], Siegfried Hapfelmeier[6], Russell G. Jones[2] and Christoph Hess[1,3,11,12]

[1] Department of Biomedicine, Immunobiology, University of Basel, 4031 Basel, Switzerland
[2] Center for Cancer and Cell Biology, Van Andel Institute, Grand Rapids, MI, USA; Goodman Cancer Research Centre, McGill University, Montreal, Quebec, Canada; Department of Physiology, McGill University, Montreal, Quebec, Canada
[3] Department of Medicine, CITIID, Jeffrey Cheah Biomedical Centre, University of Cambridge, Cambridge CB2 0AW, United Kingdom
[4] Baxter Laboratory for Stem Cell Biology, Department of Microbiology and Immunology, Stanford University School of Medicine, 269 Campus Drive, Stanford, CA 94305, USA
[5] Department of Biomedicine, Laboratory of Infection Biology, University and University Hospital Basel, 4031 Basel, Switzerland
[6] Institute for Infectious Diseases, University of Bern, 3010 Bern, Switzerland
[7] Clinical Microbiology, University Hospital Basel, 4031 Basel, Switzerland, Applied Microbiology Research, Department of Biomedicine, University of Basel, 4031 Basel, Switzerland
[8] Institute for Pathology, University Hospital Basel, University of Basel, 4031 Basel, Switzerland
[9] Department of Laboratory Medicine, University Hospital Basel, University of Basel, 4031 Basel, Switzerland
[10]Present address: Department of Diabetes, Endocrinology, Nutritional Medicine and Metabolism, Bern University Hospital, University of Bern, 3010 Bern, Switzerland and Diabetes Center Berne, 3010 Bern, Switzerland

[11]Correspondence: Maria L. Balmer (maria.balmer@unibas.ch) and Christoph Hess (chess@uhbs.ch; ch818@cam.ac.uk)
[12]Lead Contact: Further information and requests for resources and reagents should be directed to the lead contact, Christoph Hess: chess@uhbs.ch; ch818@cam.ac.uk

Summary

Serum acetate increases upon systemic infection. Acutely, assimilation of acetate expands the capacity of memory $CD8^+$ T cells to produce IFN-γ. Whether acetate modulates memory $CD8^+$ T cell metabolism and function during pathogen re-encounter remains unexplored. Here we show that at sites of infection high acetate concentrations are being reached, yet memory $CD8^+$ T cells shut down the acetate assimilating enzymes ACSS1 and ACSS2. Acetate, being thus largely excluded from incorporation into cellular metabolic pathways, now had different effects, namely (i) directly activating glutaminase, thereby augmenting glutaminolysis, cellular respiration and survival, and (ii) suppressing TCR-triggered calcium-flux, and consequently cell activation and effector cell function. *In vivo*, high acetate abundance at sites of infection improved pathogen clearance while reducing immunopathology. This indicates that, during different stages of the immune response, the same metabolite – acetate – induces distinct immunometabolic programs within the same cell type.

Introduction

Memory $CD8^+$ T cells are a small population of long-lived immune cells with protective function and unique metabolic characteristics. Effector memory (EM) $CD8^+$ T cells circulate between the blood and the periphery and migrate into various peripheral tissues, where they are exposed to constantly changing microenvironments. At tissue-sites, EM $CD8^+$ T cells rapidly respond upon re-encounter of cognate antigen by producing pro-inflammatory cytokines and other effector molecules (Harty and Badovinac, 2008). During differentiation from naïve to effector to memory cells, $CD8^+$ T cells undergo important metabolic changes, which have been intimately linked to their functional properties.

Immune cells are able to respond to their environment and acquire a variety of context-dependent fates. However, we are only beginning to understand how immune cells sense these environmental cues, and how this impacts immune cell metabolism and function. Previously we observed that systemic acetate levels rapidly increase upon infection in mice, and that, acutely, acetate at 'stress levels' enhances the glycolytic capacity and effector function of EM $CD8^+$ T cells upon subsequent re-stimulation in low acetate abundance (Balmer et al., 2016). Mechanistically, in the acute scenario acetate is assimilated via acetyl-CoA synthetase 2 (ACSS2), and is expanding the cellular acetyl-CoA pool in an ATP-citrate lyase (ACLY) dependent manner, providing acetyl-groups for acetylation reactions. Acetylation of GAPDH increases its enzymatic activity, leading to increased glycolytic activity upon activation, and augmented EM $CD8^+$ T cell effector function. Consistent with this finding, another report recently found an improved response to influenza infection in mice fed a high-fiber diet. In this experimental system, diet-derived short-chain fatty acids (SCFAs), including acetate, enhanced cellular metabolism of $CD8^+$ T cells, thereby boosting anti-viral activity (Trompette et al., 2018).

To redirect immune cells to sites of infection, chemokine gradients are established and modulate lymphocyte trafficking (Kunkel and Butcher, 2002). Several metabolites also guide lymphocyte migration (Sigmundsdottir and Butcher, 2008), such as sphingosine-1-phosphate (Pappu et al., 2007), retinoic acid (Iwata et al., 2004; Svensson et al., 2008) or vitamin D3 (Reiss et al., 2001).

Metabolites, including acetate, may therefore be viewed as carrying information that can alter immune cell function. Whether, in extension of this concept, metabolites impact immune cell function according to the stage of an evolving immune response has not been explored. Here we extended our study of acetate acutely and transiently accumulating in the blood circulation to its role at sites of prolonged inflammation in murine and human memory $CD8^+$ T cells.

Results

Acetate-levels are increased up to 100-fold at sites of infection and suppress ACSS1 and ACSS2 expression in CD8$^+$ T cells

Acetate rapidly accumulates in the circulation upon systemic infection in mice (Balmer et al., 2016). Several studies have shown dramatic changes in many metabolites in the setting of infection (Nguyen et al., 2015; Beisel, 1975; Dong et al., 2012). Here, we found that acetate accumulated in the peritoneal cavity of mice infected with *Listeria monocytogenes*, in a *Staphylococcus aureus* tissue-cage infection model, as well as in humans at sites of bacterial infection and inflammation (**Figure 1A**-**C**, **Table 1**). We next assessed how increased local acetate levels *per se* impacted numbers of memory CD8$^+$ T cells in the peritoneal cavity. To this end, mice previously infected with *Listeria monocytogenes* expressing an OVA-peptide (LmOVA) were injected intra-peritoneally (i.p.) with 10 mM acetate. Twenty-four hours after acetate injection, peritoneal CD8$^+$ T cell numbers in acetate treated mice were significantly increased as compared to mice injected with PBS (**Figure 1D**). Most of these cells expressed phenotypic markers of memory CD8$^+$ T cells (**Figure S1A**). Re-challenging these mice i.p. in presence *vs.* absence of i.p.-applied acetate, also resulted in a significant acetated-dependent increase of CD8$^+$ T cells in the peritoneal fluid (**Figure 1E**). To assess the relation between *in vivo* accumulation of acetate at sites of inflammation and CD8$^+$ T cell counts, we analyzed left-over human fluid samples collected for clinical indications, as well as murine *Staphylococcus aureus* tissue-cage fluids. In both, human and murine samples, CD8$^+$ T cell numbers and acetate abundance correlated positively up to approximately 100 mM. Beyond 100 mM of acetate, CD8$^+$ T cell numbers started to decline (**Figure 1F**,**G**). More than 60% of the CD8$^+$ T cells recovered from tissue-cage fluid had a memory phenotype (**Figure S1B**). We then asked what the metabolic consequences of exposure to increased acetate abundance at sites of inflammation might be on CD8$^+$ T cells. Specifically, we tested how ACSS1 and ACSS2 were impacted in CD8$^+$ T cells 24 h after i.p. injection of 100 mM of acetate, as well as 24 h after i.p. re-challenge of mice previously infected with LmOVA. In both models, transcript abundance of the acetate assimilating enzymes was reduced by approximately 50% (**Figure 1H**,**I**). Memory-like CD8$^+$ T cells can be generated *in vitro*, using an established protocol (**Figure S1C**) (van der Windt et al., 2012; Balmer et al., 2016). In such *in vitro* generated murine memory OT-I T cells, already after 4 h of acetate exposure, reduced abundance of ACSS1 and ACSS2 mRNA started to become apparent (**Figure S1D**-**E**). At the site of infection, cognate memory CD8$^+$ T cell activation occurs. We therefore also probed the effect of antigen-specific activation of murine memory OT-I T cells on transcript abundance of ACSS1 and ACSS2, *in vitro*. Both transcripts were strongly suppressed upon cognate re-stimulation (**Figure 1J**,**K**). Similar findings were made when activating human effector memory CD8$^+$ T cells in presence of acetate (**Figure S1F**,**G**).

In all, these data identified high levels of acetate at sites of inflammation/infection, positively correlating with increased $CD8^+$ T cells counts up to 100mM. We previously reported that acetate rapidly increased in the circulation of infected mice, and that, acutely, memory $CD8^+$ T cells assimilate acetate in an ACSS2-dependent manner – which leads to catalyzed glycolysis and increased IFN-γ production (Balmer et al., 2016). We now find that exposure of $CD8^+$ T cells to ~~further~~ increased acetate concentrations – which we show to occur at sites of infection/inflammation – evoked downregulation of ACSS1 and ACSS2, a phenomenon further accentuated by TCR activation. The experimental set-up capturing these scenarios – which, *in vivo*, plausibly form a continuum – are summarized in **Figure 1L**.

Acetate promotes glutaminolysis by enhancing glutaminase enzymatic activity

To further dissect the metabolic profile of memory $CD8^+$ T cells exposed to increased acetate levels at sites of infection, we analyzed murine memory OT-I T cells in a metabolic flux analyzer. Supplementation of acetate resulted in a significant increase in oxygen-consumption rates (OCR) compared to medium control, whereas glycolysis was unchanged (**Figure 2A** and **Figure S2A**). Furthermore, re-stimulation of memory OT-I T cells with OVA-peptide in presence of acetate also increased OCR when compared to medium control (**Figure S2B**). Addition of ^{13}C-acetate to memory OT-I T cells revealed that carbon derived from labelled acetate was found in only low amounts in citrate of memory cells stimulated with OVA (**Figure 2B**, left panel). Albeit only low in abundance also in non-activated cells, acetate-derived carbons were consistently reduced also in other intermediates of the TCA cycle (**Figure 2B**, right three panels). Of note, also expansion of acetate-fueled acetyl-CoA was much reduced upon OVA-activation of memory $CD8^+$ T cells (**Figure 2C**). These data indicated that (i) acetate assimilation was blunted in these re-stimulated memory cells, and (ii) increased OCR was not primarily resulting from increased fueling of acetate into the TCA-cycle **(Figure 2D)**. We noted, however, that the presence of acetate was associated with a higher overall abundance of α-ketoglutarate, fumarate and malate, hinting at the possibility of glutaminolysis derived glutamate as a carbon-source entering the TCA-cycle (**Figure 2B**,**D**). To test this hypothesis, ^{13}C-glutamine tracing experiments were performed, which confirmed an increase of glutamine-derived carbons in glutamate (m+5) in the presence of acetate, both in non-activated and re-stimulated murine memory $CD8^+$ T cells (**Figure 2E**, **Figure S2C**). This suggested that in this scenario acetate promoted increased glutaminolysis, TCA activity, and interlinked oxidative phosphorylation in memory $CD8^+$ T cells. Indeed, BPTES, an inhibitor of glutaminolysis, suppressed acetate-augmented OCR in murine and human memory $CD8^+$ T cells (**Figure 2F** and **Figure S2D**). BPTES alone, as well as inhibition of ATP-citrate lyase did not affect OCR (**Figure S2E**,**F**). Notably, addition of acetate up to a concentration of 50-100 mM increased human and murine $CD8^+$ T cell viability (**Figure 2G**, **Figure S2G**), a feature that was lost in absence of glutamine in the cell culture medium (**Figure 2H**, **Figure S2H**), or in presence of BPTES (**Figure S2I**). These data indicated that acetate-augmented glutaminolysis promoted

increased cell respiration and viability. At sites of high acetate concentration *in vivo*, altered migratory behavior could further contribute to increased $CD8^+$ T cell numbers. We therefore also assessed spontaneous as well as CXCL12-directed migration of murine memory OT-I T cells in presence or absence of acetate in transwell assays. In a dose dependent manner, acetate inhibited spontaneous migration compared to medium control (**Figure 2I**), and also somewhat blunted their chemokine-directed translocation (**Figure 2J**). These experiments indicated that, rather than being assimilated by members of the ACSS-family and entering core metabolism, or providing acetyl-groups for acetylation reactions (Comerford et al., 2014; Balmer et al., 2016), at the site of infection acetate modulated cellular metabolism, survival and migration in a different way.

To elucidate how acetate mediated increased glutaminolysis in memory $CD8^+$ T cells, we measured expression of glutaminase (GLS), which converts glutamine to glutamate. Addition of acetate did not change overall abundance of GLS transcript or protein (**Figure S2J**-**L**). By contrast, glutaminase activity was significantly increased in memory $CD8^+$ T cells exposed to acetate (**Figure 2K**). To dissect whether the acetate-mediated increase in glutaminase activity was a direct or indirect effect, we analyzed the activity of recombinant human glutaminase in presence *vs.* absence of acetate. These experiments revealed a direct and dose dependent effect of acetate on glutaminase-activity (**Figure S2M**), which is in line with a previous publication proposing an increase in glutaminase-activity by direct binding of acetate to the enzyme (O'Donovan and Lotspeich, 1966). To rationalize this pharmacological effect, we used *in silico* ligand docking of acetate into human glutaminase co-crystalized with bound glutamine. This identified four closely located docked-pose clusters, three of which lay close to the activation loop and one close to the substrate binding pocket (**Figure 2L**, upper panel). Of these, clusters I and II contained the greatest number of energetically favorable poses (7/10) and predicted interactions with residues that are known to affect the actions of other allosteric activators (Ferreira et al., 2013; Li et al., 2016). For example, the allosteric activator phosphate is similarly located in the mouse apo structure and its actions are strongly affected by mutation of residues G320 (G315 in 3VP0) and K325 (K317 in 3PV0) in humans (**Figure 2L**, middle panel) (Ferreira et al., 2013; Li et al., 2016). *E. coli* and *B. subtilis* both display poor amino acid conservation in this region of the enzyme and would be predicted not to be affected by acetate (**Figure 2L**, lower panel). When tested we found that, indeed, acetate did not enhance *E. coli* glutaminase activity but even decreased it (**Figure S2N**) (Brown et al., 2008; Stalnecker et al., 2017). To test, at the molecular level, the requirement of K317 for acetate to function as allosteric activator (**Figure 2L**, middle and lower panel), wild type recombinant human glutaminase (2 versions: one commercially available, one mutation-experiment control) and K317->A317 mutated recombinant glutaminase were used. Again, activity of wild type glutaminase was augmented by addition of acetate (20 mM), whereas K317->A317 mutated glutaminase was unaffected – establishing essentiality of K317 for acetate's activity augmenting property (**Figure 2M**). In all these data indicated that, upon

recall, acetate promoted glutaminolysis by direct allosteric effects that increase glutaminase activity.

Acetate suppresses TCR-re-stimulation by reducing calcium-flux

We next wondered how differential acetate handling of memory $CD8^+$ T cells re-engaging with cognate antigen related to their functionality. To begin to address this question, memory OT-I T cells were re-stimulated with OVA-peptide in presence/absence of acetate, and calcium-flux was measured by flow-cytometry. Acetate significantly suppressed calcium-flux upon OVA re-stimulation in a dose-dependent manner (**Figure 3A**), suggesting decreased TCR-stimulation. Accordingly, glycolytic switching and IFN-γ production were suppressed in presence of acetate in a dose-dependent manner in both murine and human memory $CD8^+$ T cells (**Figure 3B**-**F**), whereas production of TNF was unchanged (**Figure S3A**). Notably, calcium add-back was able to correct acetate-mediated suppression of IFN-γ (**Figure S3B**). We reasoned that negatively charged acetate may interfere with biologically active (i.e. free) calcium, which would provide a mechanistic basis to the observed effect of acetate on calcium-flux. We thus measured free calcium levels in the absence and in increasing concentrations of acetate, *in vitro*. To exclude protein-modifications by acetate, we used PBS as solute. In effect, free calcium-levels dropped in presence of acetate in a concentration-dependent manner (**Figure 3G**). Conversely, phosphate concentrations significantly increased (**Figure 3H**). To assess whether acetate depleted calcium-levels also *in vivo*, we determined free calcium levels in murine and human fluids sampled from infectious and inflamed sites. Calcium levels were significantly depleted in both, human infected and sterile inflamed body fluids, and infected murine peritoneal fluids in presence of acetate (**Figure 3I**,**J**). Inversely, phosphate-levels were increased in murine *S. aureus* skin infection and in inflamed human body fluids (**Figure 3 K**,**L**). To elucidate whether decreased calcium levels were responsible for reduced calcium-flux upon TCR re-stimulation, we added excess calcium to acetate-exposed memory OT-I T cells upon OVA re-stimulation. Addition of 10 mM calcium was sufficient to normalize calcium-flux back to control conditions (**Figure 3M**, **Figure S3C**). Addition of 10 mM calcium was also sufficient to augment memory OT-I T cell migration, indicating that impaired cell activation and migration in presence of acetate may be related to calcium-depletion in the presence of acetate (**Figure S3D**). Of note, also in absence of glutamine, acetate reduced IFN-γ production by memory OT-I T cells, indicating that the effect of acetate on glutaminase-activity and its effect on calcium-flux are distinct (data not shown). These data established that acetate suppressed memory $CD8^+$ T cell re-call responses as a consequence of reduced calcium availability when present during re-stimulation. To directly capture acetate's time- and concentration dependent immune augmenting *vs.* immuno-suppressive features, a time course experiment encompassing both features of this metabolite was performed (**Figure 3N**).

Acetate suppresses immunopathology at sites of infection and modulates tissue-remodeling

We went on and asked how, at the site of infection, acetate-mediated metabolic and functional re-programming of memory $CD8^+$ T cells modulated immune-control. To address this question, we re-infected mice, previously infected with LmOVA, i.p. in presence or absence of 10 mM acetate also administered i.p. at the same time as the pathogen. Similar to our previous findings, acetate promoted superior immune-control as measured by bacterial loads in the liver and in the spleen (**Figure 4A**). However, immunopathology determined by local lactate dehydrogenase-levels, as well as peritoneal IFN-γ, was suppressed in presence of acetate (**Figure 4B**,**C**). Peritoneal concentrations of IL-10 tended to be elevated in presence of acetate, indicating a possible immunomodulatory role of acetate (**Figure S4A**). Increased expression of PD-L1 on $CD8^+$ T cells recovered from peritoneal fluid would also align with this notion (**Figure S1A**). Histologically, peritoneal thickness – as another measure of immunopathology (Mizuno et al., 2009) – was also reduced in presence of acetate (**Figure 4D**). To further characterize a potential immunomodulatory role of acetate at the site of infection, we performed a PCR-array from peritoneal tissue of mice re-challenged with LmOVA in presence or absence of acetate. This experiment revealed increased TGF-β transcript levels in the peritoneum from acetate treated mice, whereas transcripts of the pro-inflammatory cytokines *Ifng*, *Tnf*, as well as transcripts of integrin- and collagen-family genes were decreased in presence of acetate (**Figure 4E** and **Figure S4B**). Overall, these experiments suggested that, at the site of infection, acetate suppressed immunopathology.

Taken together, our data indicated that at sites of infection acetate catalyzed glutaminolysis in memory $CD8^+$ T cells, augmenting mitochondrial respiration and cell survival. Further, by altering availability of free calcium, acetate suppressed TCR-triggered calcium-flux, glycolytic switching and IFN-γ production. In a time-resolved manner, acetate's glycolysis boosting capacity (Balmer et al., 2016) and the herein described effects were balancing pathogen clearance against immunopathology (**Figure 4F**).

Discussion

The metabolic environment has been shown to critically impact the outcome of immune responses. Probably the best characterized example is the tumor microenvironment which shapes immune cell metabolism and function. Here we show that acetate levels accumulate at sites of infection and reprogram memory $CD8^+$ T cell metabolism and function by boosting glutaminolysis and altering availability of calcium. Acetate levels can rise up to about 5 mM in the circulation upon systemic bacterial infection in mice (Balmer et al., 2016). At the site of infection, acetate levels are initially low but then can reach >100 mM. This implies that memory T cells are exposed to rising acetate concentrations at inflamed sites where they are likely to re-encounter antigen. While acute, transient exposure of ACSS competent memory $CD8^+$ T cells to acetate levels of 5 mM boosted glycolysis and cytokine secretion (Balmer et al., 2016), acetate also mediated a decrease of its assimilation machinery (i.e. ACSS1 and 2). Non-metabolized acetate on the one hand augmented glutaminase enzymatic activity, fueling the TCA-cycle and mitochondrial respiration, thereby supporting cell viability. On the other hand, acetate present during antigen re-encounter reduced free calcium abundance, thus suppressing migration and TCR-triggered calcium flux, and subsequent effector function. This indicates that, before reaching the site of infection, memory $CD8^+$ T cells are boosted and thus prepared for rapid pathogen removal at acutely infected sites (Balmer et al., 2016). However, at the site of unresolved inflammation where acetate abundance is steadily increasing, their inflammatory capacity is gradually being suppressed – thereby balancing pathogen clearance and immunopathology. Depending on timing of exposure, the same metabolite – acetate – thus has opposing effects on memory $CD8^+$ T cells: in transit to the site of infection acetate is used to acetylate and catalyze GAPDH, enhancing glycolytic switch and interlinked inflammatory output of memory $CD8^+$ T cells early upon re-stimulation (i.e. when re-stimulated in low acetate abundance). At sites of prolonged inflammation, where acetate gradually accumulates, cells lose their capacity to assimilate acetate, acetate catalyzes glutaminase activity and develops suppressive capacity by 'buffering' calcium (**Figure 4F**). Mechanistically, acetate's effects on glutaminase-activity and calcium-flux are distinct. However, functionally they may well complement each other. Initially, prolonged survival allows for sufficient cell-numbers available for efficient pathogen-clearance, while later on this may support accumulation of inflammation resolving mediators.

Immunopathology plays a key role in many infectious and inflammatory diseases, contributing to morbidity and mortality. For example, during viral infections cytotoxic $CD8^+$ T cells, while effectively killing infected cells, can also cause non-specific, tissue-destructive inflammation (Rouse and Sehrawat, 2010). Likewise, immunopathology mediates autoimmune and chronic inflammatory diseases, such as inflammatory bowel disease. In the intestine, acetate-concentrations reach up to 200 mM/kg wet weight (Farrukh, 2010; Høverstad and Midtvedt, 1986), and were significantly reduced in patients with inflammatory

bowel disease, indicating that these high acetate-concentrations contribute to host-microbial mutualism and may protect from immunopathology (Farrukh, 2010).

Acetate is a short-chain fatty acid abundantly produced by the gut microbiota via fermentation of dietary fibers (Tremaroli and Bäckhed, 2012). However, also germ-free animals readily increase serum acetate-levels upon metabolic stress, indicating efficient release of acetate from endogenous sources (Balmer et al., 2016). Further, we previously demonstrated that rising systemic acetate-levels also upon systemic bacterial infection are not primarily bacteria-driven, since also systemic infection with bacteria genetically incapable for acetate-production induced stress-levels of acetate in the host (Balmer et al., 2016). The source, or sources, of increased local acetate levels observed in this study thus remain unclear. Since also at sterile inflammatory sites acetate abundance was increased, a bacterial-origin seems unlikely. Given the large amount of cell death within any inflammatory area, one possibility could be the accumulation of extracellular acetate that is released from intracellular sources upon cell death.

In conclusion, our data demonstrate that acetate can function as a rheostat of the immune response, balancing pro- and anti-inflammatory properties during the course of an immune response. Opposing effects on immune cell function driven by a single metabolite through distinct cellular metabolic effects emphasize the need to consider metabolic reprogramming in a time- and context resolved manner.

Limitations of Study

The molecular mechanisms by which acetate and TCR signaling drive downregulation of ACSS1 and ACSS2 remain to be defined. Also, we could not measure memory $CD8^+$ T cell metabolism in real time *in vivo* during the course of an infection, but focused on *ex vivo* analyses. Finally, while we found increased accumulation of acetate at sites of inflammation also in humans, how memory $CD8^+$ T cell metabolism is regulated at these sites needs to be explored.

Acknowledgements

M.L.B. was supported by SNSF Grant PMPDP3_171261/1 and Novartis Foundation Grant 17C141. C.H. was supported by SNSF Grant 31003A_172848 and 310030_192677.

Author contributions

M.L.B. designed, performed and analyzed most experiments and wrote the manuscript, E.H.M. and R.G.J. performed metabolic tracing experiments, A.T. performed *in silico* docking experiments, R.E. performed experiments and analyzed data, G.U. performed immunoblot analyses, J.Loet. performed calcium-flux experiments, P.D. performed migration experiments, C.M.S. examined and scored the histopathological samples, J.D.W. performed immunoblot, RT-PCR, migration and calcium-flux experiments, G.P. and G.R.B. established glutaminase-activity assays, A.W., J.G. and N.K. performed MSSA tissue cage experiments, A.E. and L.B. provided clinical samples for acetate measurements, K.R. measured calcium and phosphate concentrations, J.Loel. and N.A. helped with metabolic tracing experiments, O.S. and S.H. performed PCR-Arrays, C.H. designed, supervised and coordinated the study and wrote the manuscript. All authors revised the manuscript and approved its final version.

Declaration of interests

The authors declare no conflict of interest.

Figure legends

Figure 1: *Acetate-levels are up to 100-fold increased at sites of infection and suppress ACSS1 and ACSS2 expression in CD8⁺ T cells.* **A**) Acetate levels in the peritoneal fluid, 24 h after i.p. LmOVA-infection in C57BL/6 mice. **B**) Acetate levels in tissue cages at the indicated time-points following *S. aureus* infection. **C**) Acetate levels in human infected body fluids (abscesses) as compared to non-inflamed control fluids. **D**) $CD8^+$ T cell numbers in the peritoneal fluid 24 h upon i.p.-administration of 10 mM acetate in LmOVA-immunized mice. **E**) $CD8^+$ T cell numbers in the peritoneal fluid 24 h upon i.p. re-infection with LmOVA +/- 10 mM acetate in LmOVA-immunized mice. **F** and **G**) Absolute numbers of $CD8^+$ T cells recovered from locally infected fluids shown in (**B**) and (**C**) as determined by flow cytometry. **H** and **I**) Expression of ACSS1 and ACSS2 in MACS-purified $CD8^+$ T cells from the peritoneal cavity of LmOVA-immunized mice upon injection of 100 mM acetate (**H**) or re-challenged with LmOVA (**I**). **J** and **K**) Expression of ACSS1 (**J**) and ACSS2 (**K**) in murine memory OT-I T cells upon OVA-stimulation for 4 h in presence or absence of the indicated acetate-concentrations. **L**) Experimental set-up mimicking the time-course of acetate-exposure of memory $CD8^+$ T cells. Each dot represents one mouse or sample, lines indicate means. Error bars are SD. Dashed lines indicate the detection limit. T-test (**A**, **C**, **D**, **E**), One-way ANOVA (**B** and **F**) and Two-way ANOVA (**H-K**) were used to compare the groups. * $P < 0.05$, ** $P < 0.01$, **** $P < 0.0001$

Figure 2: *Acetate promotes glutaminolysis by enhancing glutaminase enzymatic activity.* **A**) Memory OT-I T cells were analyzed by metabolic flux analysis upon injection of 5 mM acetate (blue) or medium control (black) at the beginning of the analysis (dashed line and arrow). Shown is a representative experiment of OCR-values and pooled data from 5 independent experiments showing OCR-values at 300 min post-injection. **B** and **C**) ^{13}C-acetate tracing experiment of murine memory OT-I T cells. Cells were incubated +/- 5 mM ^{12}C-acetate (blue) and +/- 10 µM OVA-peptide for 6 h and then all traced with ^{13}C-acetate for 6 h. **B**) Filled bars represent contribution of ^{13}C-acetate to the respective metabolite-pool. **C**) Relative abundance of m+2 acetyl-CoA from ^{13}C-acetate. **D**) Schematic of mitochondrial metabolism and possible effects of acetate. **E**) Same experiment as in (**B**), but with ^{13}C-glutamine. The different colors indicate the number of radiolabeled carbons detected in glutamate. **F**) Memory OT-I T cells were pre-incubated for 2 h in presence (red) or absence (black) of the glutaminolysis-inhibitor BPTES or vehicle control. Cells were then analyzed by metabolic flux analysis upon injection of 5 mM acetate (dashed line and arrow). Shown is a representative experiment of OCR-values and pooled data from 4 independent experiments assessing the net-increase in OCR between time-point 30 and 150 min. **G** and **H**) Viability of murine memory $CD8^+$ T cells cultured *in vitro* for 3 days in presence (**G**) or absence (**H**) of glutamine and increasing acetate-concentrations as determined by flow cytometry (% Annexin V and PI negative). **I** and **J**) Spontaneous (**I**) and chemokine-directed (**J**) migratory capacity of *in vitro* generated murine memory OT-I T cells analyzed in a transwell-assay in increasing

concentrations of acetate. **K**) Glutaminase activity in murine memory OT-I T cell extracts exposed for 4 h to the indicated acetate-concentrations. **L**) Upper panel: a wireframe representation of the four docked pose clusters identified in our study is shown in one of the four subunits of the enzymatically active homo-tetramer of glutaminase. Middle: An example docked-pose from cluster I, showing predicted hydrogen bond interactions (dashed orange lines) between acetate and the side chains of residues S319 (314) and K235 (317). The green molecule is bound glutamine. Bottom: an alignment showing the poor amino acid conservation in the predicted allosteric activation region of human (from the 3PV0 crystal structure used here) and prokaryotic glutaminase (P77454, *E. coli*; O31465, *B. subtilis*). The gray shade highlights S314 and K317. **M**) Glutaminase activity of human recombinant glutaminase (rh), wildtype human glutaminase (wt = mutation control) and human glutaminase with a K->A mutation at position 317, depicted in the lower panel of (**L**), assessed in presence or absence of 20 mM acetate.

Each dot represents one mouse or human, lines indicate means, error bars are SD. T-test (**A**, **F**), One-way ANOVA (**G**, **H**, **I**, **K**) or Two-way ANOVA (**B**, **C**, **J**, **M**) were used to compare the groups. * $P < 0.05$, ** $P < 0.01$, *** $P < 0.001$, **** $P < 0.0001$

Figure 3: *Acetate suppresses TCR-re-stimulation by reducing calcium availability.* **A**) Calcium flux as assessed by flow cytometry of murine memory OT-I T cells cultured in presence (blue) or absence of acetate (black) for 30 min. One representative experiment (left) and pooled data from 2-3 independent experiments (right) are shown. **B**) Glycolytic switch upon OVA-injection with (blue) or without (black) acetate in murine memory OT-I T cells as assessed by metabolic flux analysis. One representative experiment (left) and pooled data from 4 independent experiments (right) are shown. The glycolytic switch was calculated by subtracting the basal ECAR from maximal ECAR. The dashed line indicates the time of OVA (+/- acetate) injection. **C** and **D**) IFN-γ production as assessed by intracellular cytokine staining in murine (**C**) or human (**D**) memory $CD8^+$ T cells 4 h after re-stimulation with 10 µM OVA-peptide or anti-CD3/CD28 antibodies in presence (blue) or absence (black) of indicated acetate-concentrations. **E** and **F**) IFN-γ mRNA (**E**) and protein (**F**) in human memory $CD8^+$ T cells 4 h after re-stimulation with anti-CD3/CD28 antibodies in presence (blue) or absence (black) of indicated acetate-concentrations. **G** and **H**) Calcium- (**G**) and phosphate-levels (**H**) assessed *in vitro* in presence (blue) or absence (black) of the indicated acetate-concentrations. **I**-**K**) Calcium- (**I** and **J**) and phosphate-levels (**K** and **L**) in human and murine fluids as described in Figure 1A-C. **M**) Calcium-flux as described in (**A**) was assessed in presence (blue) or absence (black) of acetate and additional calcium. **N**) IFN-γ production as assessed by intracellular cytokine staining in murine memory OT-I T cells either exposed to acetate prior or during OVA-re-stimulation for 4 h.

Each dot represents one mouse or human, lines indicate means, error bars are SD. T-test (**B**, **I**, **J, L**), One-way ANOVA (**G**, **H**, **K**, **M, N**) or Two-way ANOVA (**C**-**F**) were used to compare the groups. * $P < 0.05$, ** $P < 0.01$, *** $P < 0.001$, **** $P < 0.0001$

Figure 4: *Acetate suppresses immunopathology at sites of infection and modulates tissue-remodeling.* **A**) LmOVA-immunized mice were i.p. re-infected with 10^5 CFU LmOVA in presence (blue) or absence (black) of 10 mM acetate and bacterial burdens in spleen and liver were assessed by bacterial plating 24 h post-infection. **B**) LDH levels in the peritoneal fluid of mice described in (**A**) were analyzed using a commercially available assay kit. **C**) IFN-γ levels in the peritoneal fluid of mice described in (**A**) were determined by cytometric bead array. **D**) Peritoneal morphology on formalin-fixed, paraffin-embedded samples stained with elastica van Gieson. Shown are representative samples of one control (Ctr) and one acetate-treated (Ac) animal. Peritoneal thickness was quantified (right panel). **E**) Volcano plot of PCR-array analysis of the peritoneal samples shown in (**D**). Red-highlighted genes were upregulated, green-highlighted genes down-regulated in presence of acetate. **F**) Schematic depiction of the proposed model of acetate, playing opposing roles during an immune response in a time and context dependent manner.

Each dot in A-D represents one mouse. Shown are pooled data from 2 independent experiments with 3-7 animals per group. Lines indicate means, error bars are SD. Dashed lines in A and C indicate the detection limit. T-test was used to compare the groups. * $P < 0.05$, ** $P < 0.01$

Table 1: Patient characteristics

Gender (f/m)	6 / 5
Age (mean, years)	51
Source (n)	
abscess/cyst	7
wound	1
ascites	1
synovia	2
Pathogen isolated (n)	
Staphylococcus aureus	1
Staphylococcus epidermidis	1
mixed	4

RESOURCE AVAILABILITY

Lead Contact

Further information and requests for resources and reagents should be directed to and will be fulfilled by the Lead Contact, Christoph Hess (ch818@cam.ac.uk; chess@uhbs.ch).

Materials Availability

This study did not generate new unique reagents.

Data and Code Availability

The published article includes all datasets generated or analyzed during this study.

EXPERIMENTAL MODEL AND SUBJECT DETAILS

Animal husbandry

Male and female C57BL/6 or MHC class I-restricted OVA-specific T cell receptor (OT-I) transgenic mice were 6-8 weeks of age and housed in IVC cages on racks in a room with controlled temperature (22-24°C) and humidity (40-60%). Mice were maintained on a 12 hour light-dark cycle. All mice were fed a standard diet (Kliba AG, #3436 EX). Health checks were conducted on all mice at least once daily. For experimental control groups, littermates were used. All animal experiments were approved by the Animal Care Committee of the Veterinary Office Basel, Switzerland.

Human abscess fluids

Human abscess fluids were obtained from the division of Clinical Microbiology of the University Hospital Basel after informed consent of the patients and ethical approval of the ethics committee of both Basels. As controls, non-inflamed samples (e.g. sterile ascites, cyst-fluids, pleural transudate) were used. Samples were stored at 4°C prior to measurement. Patient characteristics are summarized in **Table 1**.

Isolation of human effector memory (EM) $CD8^+$ T Cells

Peripheral blood mononuclear cells were isolated by standard density-gradient centrifugation protocols (Lymphoprep; Fresenis Kabi) from healthy male and female blood donors, >18 years of age. Results were not stratified by age or sex, since we did not have this information at the time of analysis. MACS beads and LS columns (both Milteny Biotec) were used to sort $CD8^+$ positive T cells. The positively selected $CD8^+$ T cells were incubated with APC anti-CD62L mAb (ImmunoTools) and Pacific Blue anti-CD45RA (Beckman Coulter) and sorted by flow cytometry (BD FACSAria III or BD Influx Cell Sorter). Experiments using blood donor derived cells were approved by the blood transfusion service of the Swiss Red Cross.

Cell culture

Primary cells of male and female mice were cultured in RPMI medium (RPMI 1640 containing 10% FCS, 100 U/mL penicillin, 100 µg streptomycin, 0.29 mg/mL L-glutamine, 50 µM 2-Mercaptoethanol) at 37°C and 5% CO2.

METHOD DETAILS

In vitro memory differentiation

Memory OT-I T cells were generated as described previously (Balmer et al., 2016; van der Windt et al., 2013). Briefly, the lymph nodes from MHC class I-restricted OVA-specific T cell receptor (OT-I) transgenic mice and the spleen of C57BL/6 mice were aseptically removed and incubated in liberase TL (Roche) for 30 min. After mashing through a 70 µm cell strainer (BD Biosciences), red blood cells were lysed with RBC Lysis Buffer Solution (eBioscience). The isolated cell suspensions were washed in RPMI medium (RPMI 1640 containing 10% FCS, 100 U/mL penicillin, 100 µg streptomycin, 0.29 mg/mL L-glutamine, 50 µM 2-Mercaptoethanol (Life Technologies)) and re-suspended to 10^6 cells/ml. The splenocytes and OT-I cells were pooled in a ratio of 1:1 and activated with OVA peptide (Eurogentec) at 10^{-9} M at 37°C for 3 days. The cells were then washed and re-suspended to 2 x 10^6 cells/ml and cultured in the presence of IL-15 (10 ng/ml) at 37°C for another 3 days to generate OVA-specific memory $CD8^+$ T cells. Phenotyping was performed using BUV395-anti CD44 (BD), APC-anti CD8, BV421-anti KLRG1, PE-anti-CD62L, APC-Cy7-anti CD43, BV421-anti PDL1, PE-anti-CD25, BV510-anti CD27 (all Biolegend) and PE-Cy5-anti CD127 (eBioscience).

Acetate measurement in murine and human samples

Acetate concentrations in peritoneal fluids and human samples were determined using the acetate fluorimetric assay kit (Bioassay Systems), following the manufacturer's instructions.

Measurement of cell viability

To measure the viability, 10^5 mouse or human memory $CD8^+$ T cells were plated in a 96-well plate in RPMI medium. The cells were incubated at 37°C for up to 7 days. The cells were washed in Annexin V Binding Buffer (BD Pharmingen) and stained with APC Annexin V (ImmunoTools) and PI (Sigma Aldrich). Samples were acquired on an Accuri® C6 Flow Cytometer and analyzed with FlowJo-Software (FlowJo 10.2). Viable cells were defined as Annexin V and PI double negative. Where indicated, cells were incubated in presence of BPTES (Sigma Aldrich) at 50 µM or in glutamine-free RPMI containing dialyzed FCS (Life Technologies).

Transwell migration assay

For the *in vitro* migration assay 2-5 x 10^5 cells were resuspended in 80% full medium and 20% PBS, supplemented with varying concentration of sodium acetate, calcium chloride and sodium chloride. 100 µL of cell suspension was seeded in 5 µm pore cell culture inserts (Sigma, CLS3421) with 500 µL of the corresponding medium in the well. After 3 h incubation at 37°C, the volumes in the insert and the well were measured with a pipette. The cell density was

measured by acquiring 30 µL of the insert and well with a CytoFlex flow cytometer (Beckman Coulter) by counting the number of events in the live gate using FlowJo. The translocation index was calculated by dividing the cell number of the cell culture insert with the total cell number. Every condition was assessed by technical triplicates and every experiment was repeated at least three times. Where indicated, CXCL12 (Peptrotech) at 50 ng/ml was used.

Murine peritonitis model

C57BL/6 mice were intra-peritoneally (i.p.) infected with 5000 CFU *Listeria monocytogenes* expressing the OVA-peptide (LmOVA). 28 days later, mice were re-infected with 10^5 CFU LmOVA i.p. in presence or absence of 5 mM acetate. Mice were sacrificed 24 h later and peritoneal fluid, spleen, liver and serum harvested. Spleens and livers were homogenized in 0.5% Terigitol/PBS using a Tissuelyser (Qiagen) and sterile stainless-steel ball bearings. Organ suspensions were then plated on BHI agar-plates and colonies counted upon 24 h incubation at 37°C. Peritoneal fluids were centrifuged and the cells analyzed by flow-cytometry upon staining with FITC-anti-CD3, BUV395-anti CD44 (both BD), BV421-anti PDL1, APC-Cy7-anti CD43, BV510-anti CD27 and PE-anti CD8 antibodies, Zombie-Red viability staining (all Biolegend) or by RT-PCR upon MACS-purification and storage in Trizol Reagent (Thermo Fisher Scientific). Peritoneal fluids and sera were frozen at -80°C prior to further analysis. LDH concentrations in peritoneal fluids were measured using a commercially available assay kit (Abcam). All experiments were performed in accordance with local rules for the care and use of laboratory animals.

S. aureus tissue cage model

The mouse model of foreign-body infection (John et al., 2011; Nowakowska et al., 2014) was used in the present study. Briefly, a sterile tissue cage (Angst + Pfister AG, Zurich, Switzerland) was implanted subcutaneously in the back of female C57BL/6 mice, 13 weeks old (janvierlab, France). After complete wound healing (2 weeks), cages were tested for sterility by culturing the aspirated tissue cage fluid (TCF). Teflon cages were infected with 785 CFU of MSSA ATCC 29213. The infection was confirmed at day 1 directly before treatment start by plating. Mice were i.p. treated twice a day with 5% glucose for 11 days. Tissue cage fluid (TCF) was aspirated at different time points (day 3, 6, 9, 11 and 14) and apropriate dilutions were plated to determine the amount of planktonic MSSA. Tissue cage fluids were then analyzed for acetate, calcium and phosphate levels and $CD8^+$ T cells isolated by MACS-purification and frozen in Trizol Reagent (Thermo Fisher Scientific). For phenotyping, cells were stained with APC-anti CD8 (Biolegend), BUV395-anti CD44 (BD), PE-anti CD62L (Biolegend) antibodies and Zombie-Red Viability staining (Biolegend).

Histology

Small pieces (0.5 x 0.5 cm) of peritoneum were fixed in 4% formaldehyde for 24 h. Samples were then paraffin-embedded, cut, and stained with H&E and elastica van Gieson on an automated-stainer according to standard procedures. Peritoneal thickness was measured

from the mesothelial surface to the border of the loose connective tissue between compact zone and muscular layer by a board-certified pathologist in a blinded manner as described in (Mizuno et al., 2009).

Seahorse experiments

Oxygen consumption rates (OCR, in pMoles/min) and extracellular acidification rates (ECAR, in mpH/min) were measured in plated cells (2.5 x 10^5 per well) kept in serum-free unbuffered RPMI-1640 medium (Sigma-Aldrich), under basal conditions, and in response to OVA-peptide (10 µM) or acetate (5 mM) injection using the instrument's multi-injection ports. Where indicated, cells were pre-treated with the ACLY-inhibitor SB204990 (Tocris) at 30 µM or BPTES (Sigma Aldrich) at 50 µM 2 h prior to and during metabolic flux analysis or vehicle control. All data were generated using the XF-96 Extracellular Flux Analyzer (Seahorse Bioscience).

Metabolic tracing

GC-MS metabolite analysis was conducted as previously described (Blagih et al., 2015) (Balmer et al., 2016). Briefly, 5 x 10^6 IL-15 expanded OT-I memory cells were cultured in standard or glutamine-free RPMI (with 10% dialyzed FCS) containing 10 mM 1,2-[13C]-acetate or 10 mM 13C-glutamine (Cambridge Isotope Laboratories) for 6 h. Metabolites were extracted from cells using ice-cold 80% methanol, followed by sonication and removal of cellular debris by centrifugation at 4°C. Metabolite extracts were dried, derivatized as tert-butyldimethylsilyl (TBDMS) esters, and analyzed via GC-MS as previously described (Faubert et al., 2014). Uniformly deuterated myristic acid (750 ng/sample) was added as an internal standard following cellular metabolite extraction, and metabolite abundance was expressed relative to the internal standard and normalized to cell number. Mass isotopomer distribution was determined using a custom algorithm developed at McGill University, CA (McGuirk et al., 2013).

Quantitative PCR

Quantitative PCR for mouse ACSS1 and ACSS2 mRNA was done in triplicates with SYBR Green Supermix (Promega). The following primers were used: ms ACSS1 (forward 5'-GTTTGGGACACTCCTTACCATAC-3' and reverse 5'-AGGCAGTTGACAGACACATTC-3'), ms ACSS2 (forward 5'-GTGAAAGGATCTTGGATTCCAGT-3' and reverse 5'-CAGATGTTTGACCACAATGCAG-3') (both Invitrogen). The following primers were used to analyze glutaminase mRNA: Mm01257297_m1 (Thermo Fisher Scientific). *IFNg* mRNA was measured using primers Mm01168134_m1 (Thermo Fisher Scientific). As a housekeeping gene mouse 18S mRNA was measured using ms 18S primers (forward 5'-GGGAGCCTGAGAAACGGC-3' and reverse 5'-GGGTCGGGAGTGGGTAATTT-3') (Microsynth). Quantitative PCR for human ACSS1 and ACSS2 mRNA was done in triplicates with SYBR Green Supermix (Promega). The following primers were used: hs ACSS1 (forward 5'-CACAGGACAGACAACAAGGTC-3' and reverse 5'-CCTGGGTATGGAACGATGCC-3'), hs ACSS2 (forward 5'-AAAGGAGCAACTACCAACATCTG-3' and reverse 5'-GCTGAACTGACACACTTGGAC-3') (both Invitrogen). As a housekeeping gene 18S

was used (4310893E, Applied Biosystems). Peritoneal immunopathology was assessed using the mouse Wound Healing RT^2 Profiler PCR Array following the manufacturer's instructions (Qiagen). RNA-quality was checked prior to the assay using the Bioanalyzer RNA-kit (Agilent).

Glutaminase activity assay

To analyze the activity of glutaminase in memory CD8$^+$ T cells, the Glutaminase Microplate Assay Kit (Cohesion Biosciences) was used. After incubation, cells (4 Mio) were sonicated in the assay buffer (40 µl) provided with the kit and then processed according to the manufacturer's instructions. Recombinant human glutaminase at 1 µg/ml (R&D Systems) and glutaminase from *E. coli* at 6 U/ml (Megazyme) were tested in the Glutaminase Microplate Assay (Cohesion Biosciences).

Glutaminase-acetate in silico docking

We used a template of the human glutaminase co-crystallized with bound glutamine (PDB ID 3VP0). The three-dimensional structure of acetate was constructed *ab initio* in Chem3D Pro v14.0 (CambridgeSoft, Cambridge, UK) and energy-minimized using the integrated MM2 force field. The binding site of acetate was defined as being within 20 Å of the centroid around the α-carbon of Y446, a centrally located residue that interacts with glutamine in the substrate binding site. Acetate was docked as a flexible ligand into the ligand-occupied structure using GOLD Suite v5.7.0 (The Cambridge Crystallographic Data Centre, Cambridge, UK) with the GoldScore function and default settings. Ten docked poses were generated and visualised with PyMol v1.3.

Glutaminase mutagenesis

Human GLS2 was cloned into the multiple cloning site of a pGEX-4T-1 bacterial expression vector containing a C-terminal glutathione-S-transferase (GST) tag. The K253A variant was generated by site-directed mutagenesis which corresponds to the GLS1 sequence K->A shown in **Figure 2L**. The *E. coli* strain BL21(DE3) was then transformed with wild type or K253A mutant pGEX-4T-1-GLS2 vectors. Recombinant GLS2-GST was purified from bacterial cell lysate using GST hiTRAP and Superdex 200 columns and eluted in 5mM Tris, 150mM HCl buffer (pH 7.5). Wildtype and mutant glutaminase was used at a concentration of 1 µg/ml for measuring glutaminase activity as described above.

Calcium flux

In vitro differentiated memory OT-I T cells were loaded with 1 µM Fluo4 (Invitrogen) and 1 µM Fura Red (Invitrogen) with indicated acetate or calcium concentrations for 30 min at 37°C. After washing, T cells were activated with 10 µM OVA-peptide under continuous acquisition using an Accuri C6 (BD) or Cytoflex (Beckmann coulter) flow cytometer. Analysis was performed with FlowJo software using kinetics tool (ratio of geometric mean fluorescence intensity of Fluo4/FuraRed) and Prism software.

Calcium and phosphate quantification

Calcium and phosphate concentrations were measured in collaboration with the diagnostics department of the University Hospital Basel using a fotometric Assay (Cobas, Roche). For *in vitro* calcium-measurements, PBS was supplemented with increasing concentrations of acetate and calcium-concentrations measured immediately.

Intracellular cytokine staining

200,000 cells per condition were re-activated with CD3/CD28 beads (1:10) or OVA-peptide (10 µM) in presence or absence of the indicated concentrations of acetate or calcium for 4 h. Brefeldin A (Biolegend) was added after 1 h of incubation. Fixation and permeabilization with BD Cytofix/Cytoperm™ and BD Perm/Wash™ was done according to the instruction of the manufactorer (BD Biosciences). Cells were then stained with FITC-anti-human IFN-γ (BD Biosciences) or FITC-anti-mouse IFN-γ (Biolegend), aquired on an Accuri® C6 Flow Cytometer and analyzed using FlowJo-Software (FlowJo 10.2).

Cytrometric bead array

Cytokine concentrations in cell culture supernatants and peritoneal fluids were determined using the LegendPlex cytrometric bead Array Th1-Pannel (Biolegend), according to the manufacturer's instructions.

Immunoblot analysis

Memory T cells were lysed in RIPA buffer (Thermo Scientific) containing protease- and phosphatase-inhibitors (Roche, #05 892 970 001 and #04 906 837 001), and protein concentrations determined with a BCA protein assay kit (Thermo Scientific). Whole-cell lysates were separated by 4–20% SDS-PAGE and transferred to nitrocellulose or PVDF membranes. Membranes were probed with anti-glutaminase mAb (Protein Tech, #19958-1-AP) and anti-actin mAb (Sigma #A1978). Blots were then stained with the appropriate secondary antibody (IRDye 800CW– conjugated goat polyclonal antibody to rabbit IgG (926-32211) from LI-COR). The Odyssey imaging system (LICOR) was used for detection, and the ImageJ software (1.48v) for quantification.

Quantification and statistical analysis

Differences were analyzed for statistical significance using Prism 7 for Macintosh (GraphPad Software Inc.). The details of the tests carried out are indicated in each figure legend. Where data were approximately normally distributed, values were compared using either a Student's t test, one-way or two-way ANOVA. Where data were non-normally distributed Wilcoxon-tests were applied. In all cases, p-values < 0.05 were considered significant.

REFERENCES

Balmer, M.L., Ma, E.H., Bantug, G.R., Grählert, J., Pfister, S., Glatter, T., Jauch, A., Dimeloe, S., Slack, E., Dehio, P., Krzyzaniak, M.A., King, C.G., Burgener, A.-V., Fischer, M., Develioglu, L., Belle, R., Recher, M., Bonilla, W.V., Macpherson, A.J., Hapfelmeier, S., Jones, R.G., Hess, C., 2016. Memory CD8(+) T Cells Require Increased Concentrations of Acetate Induced by Stress for Optimal Function. Immunity 44, 1312–1324.

Beisel, W.R., 1975. Metabolic response to infection. Annu. Rev. Med. 26, 9–20.

Blagih, J., Coulombe, F., Vincent, E.E., Dupuy, F., Galicia-Vázquez, G., Yurchenko, E., Raissi, T.C., van der Windt, G.J.W., Viollet, B., Pearce, E.L., Pelletier, J., Piccirillo, C.A., Krawczyk, C.M., Divangahi, M., Jones, R.G., 2015. The energy sensor AMPK regulates T cell metabolic adaptation and effector responses in vivo. Immunity 42, 41–54.

Brown, G., Singer, A., Proudfoot, M., Skarina, T., Kim, Y., Chang, C., Dementieva, I., Kuznetsova, E., Gonzalez, C.F., Joachimiak, A., Savchenko, A., Yakunin, A.F., 2008. Functional and structural characterization of four glutaminases from Escherichia coli and Bacillus subtilis. Biochemistry 47, 5724–5735.

Comerford, S.A., Huang, Z., Du, X., Wang, Y., Cai, L., Witkiewicz, A.K., Walters, H., Tantawy, M.N., Fu, A., Manning, H.C., Horton, J.D., Hammer, R.E., McKnight, S.L., Tu, B.P., 2014. Acetate dependence of tumors. Cell 159, 1591–1602.

Dong, F., Wang, B., Zhang, L., Tang, H., Li, J., Wang, Y., 2012. Metabolic response to Klebsiella pneumoniae infection in an experimental rat model. PLoS ONE 7, e51060.

Farrukh, 2010. The Impact of the Level of the Intestinal Short Chain Fatty Acids in Inflammatory Bowel Disease Patients Versus Healthy Subjects 1–6.

Faubert, B., Vincent, E.E., Griss, T., Samborska, B., Izreig, S., Svensson, R.U., Mamer, O.A., Avizonis, D., Shackelford, D.B., Shaw, R.J., Jones, R.G., 2014. Loss of the tumor suppressor LKB1 promotes metabolic reprogramming of cancer cells via HIF-1α. Proc. Natl. Acad. Sci. U.S.A. 111, 2554–2559.

Ferreira, A.P.S., Cassago, A., Gonçalves, K. de A., Dias, M.M., Adamoski, D., Ascenção, C.F.R., Honorato, R.V., de Oliveira, J.F., Ferreira, I.M., Fornezari, C., Bettini, J., Oliveira, P.S.L., Paes Leme, A.F., Portugal, R.V., Ambrosio, A.L.B., Dias, S.M.G., 2013. Active glutaminase C self-assembles into a supratetrameric oligomer that can be disrupted by an allosteric inhibitor. Journal of Biological Chemistry 288, 28009–28020.

Harty, J.T., Badovinac, V.P., 2008. Shaping and reshaping CD8+ T-cell memory. Nature Publishing Group 8, 107–119.

Høverstad, T., Midtvedt, T., 1986. Short-chain fatty acids in germfree mice and rats. J. Nutr. 116, 1772–1776.

Iwata, M., Hirakiyama, A., Eshima, Y., Kagechika, H., Kato, C., Song, S.-Y., 2004. Retinoic acid imprints gut-homing specificity on T cells. Immunity 21, 527–538.

John, A.-K., Schmaler, M., Khanna, N., Landmann, R., 2011. Reversible daptomycin tolerance of adherent staphylococci in an implant infection model. Antimicrob. Agents Chemother. 55, 3510–3516.

686 Kunkel, E.J., Butcher, E.C., 2002. Chemokines and the tissue-specific migration of
687 lymphocytes. Immunity 16, 1–4.

688 Li, Y., Erickson, J.W., Stalnecker, C.A., Katt, W.P., Huang, Q., Cerione, R.A., Ramachandran, S.,
689 2016. Mechanistic Basis of Glutaminase Activation: A KEY ENZYME THAT PROMOTES
690 GLUTAMINE METABOLISM IN CANCER CELLS. Journal of Biological Chemistry 291, 20900–
691 20910.

692 McGuirk, S., Gravel, S.-P., Deblois, G., Papadopoli, D.J., Faubert, B., Wegner, A., Hiller, K.,
693 Avizonis, D., Akavia, U.D., Jones, R.G., Giguère, V., St-Pierre, J., 2013. PGC-1α supports
694 glutamine metabolism in breast cancer. Cancer Metab 1, 22.

695 Mizuno, M., Ito, Y., Hepburn, N., Mizuno, T., Noda, Y., Yuzawa, Y., Harris, C.L., Morgan, B.P.,
696 Matsuo, S., 2009. Zymosan, but not lipopolysaccharide, triggers severe and progressive
697 peritoneal injury accompanied by complement activation in a rat peritonitis model. The
698 Journal of Immunology 183, 1403–1412.

699 Nguyen, C.T.Q., Shetty, V., Maresso, A.W., 2015. Global metabolomic analysis of a
700 mammalian host infected with Bacillus anthracis. Infect Immun 83, 4811–4825.

701 Nowakowska, J., Landmann, R., Khanna, N., 2014. Foreign Body Infection Models to Study
702 Host-Pathogen Response and Antimicrobial Tolerance of Bacterial Biofilm. Antibiotics (Basel)
703 3, 378–397.

704 O'Donovan, D.J., Lotspeich, W.D., 1966. Activation of kidney mitochondrial glutaminase by
705 inorganic phosphate and organic acids. Nature 212, 930–932.

706 Pappu, R., Schwab, S.R., Cornelissen, I., Pereira, J.P., Regard, J.B., Xu, Y., Camerer, E., Zheng,
707 Y.-W., Huang, Y., Cyster, J.G., Coughlin, S.R., 2007. Promotion of lymphocyte egress into
708 blood and lymph by distinct sources of sphingosine-1-phosphate. Science 316, 295–298.

709 Reiss, Y., Proudfoot, A.E., Power, C.A., Campbell, J.J., Butcher, E.C., 2001. CC chemokine
710 receptor (CCR)4 and the CCR10 ligand cutaneous T cell-attracting chemokine (CTACK) in
711 lymphocyte trafficking to inflamed skin. J Exp Med 194, 1541–1547.

712 Rouse, B.T., Sehrawat, S., 2010. Immunity and immunopathology to viruses: what decides
713 the outcome? Nat Rev Immunol 10, 514–526.

714 Sigmundsdottir, H., Butcher, E.C., 2008. Environmental cues, dendritic cells and the
715 programming of tissue-selective lymphocyte trafficking. Nat. Immunol. 9, 981–987.

716 Stalnecker, C.A., Erickson, J.W., Cerione, R.A., 2017. Conformational changes in the
717 activation loop of mitochondrial glutaminase C: A direct fluorescence readout that
718 distinguishes the binding of allosteric inhibitors from activators. Journal of Biological
719 Chemistry 292, 6095–6107.

720 Svensson, M., Johansson-Lindbom, B., Zapata, F., Jaensson, E., Austenaa, L.M., Blomhoff, R.,
721 Agace, W.W., 2008. Retinoic acid receptor signaling levels and antigen dose regulate gut
722 homing receptor expression on CD8+ T cells. Mucosal Immunol 1, 38–48.

723 Tremaroli, V., Bäckhed, F., 2012. Functional interactions between the gut microbiota and
724 host metabolism. Nature 489, 242–249.

725 Trompette, A., Gollwitzer, E.S., Pattaroni, C., Lopez-Mejia, I.C., Riva, E., Pernot, J., Ubags, N.,
726 Fajas, L., Nicod, L.P., Marsland, B.J., 2018. Dietary Fiber Confers Protection against Flu by

727 Shaping Ly6c- Patrolling Monocyte Hematopoiesis and CD8+ T Cell Metabolism. Immunity
728 48, 992–1005.e8.

729 van der Windt, G.J.W., Everts, B., Chang, C.-H., Curtis, J.D., Freitas, T.C., Amiel, E., Pearce,
730 E.J., Pearce, E.L., 2012. Mitochondrial Respiratory Capacity Is a Critical Regulator of CD8(+) T
731 Cell Memory Development. Immunity 36, 68–78.

732 van der Windt, G.J.W., O'Sullivan, D., Everts, B., Huang, S.C.-C., Buck, M.D., Curtis, J.D.,
733 Chang, C.-H., Smith, A.M., Ai, T., Faubert, B., Jones, R.G., Pearce, E.J., Pearce, E.L., 2013. CD8
734 memory T cells have a bioenergetic advantage that underlies their rapid recall ability. Proc.
735 Natl. Acad. Sci. U.S.A. 110, 14336–14341.

Figure 1

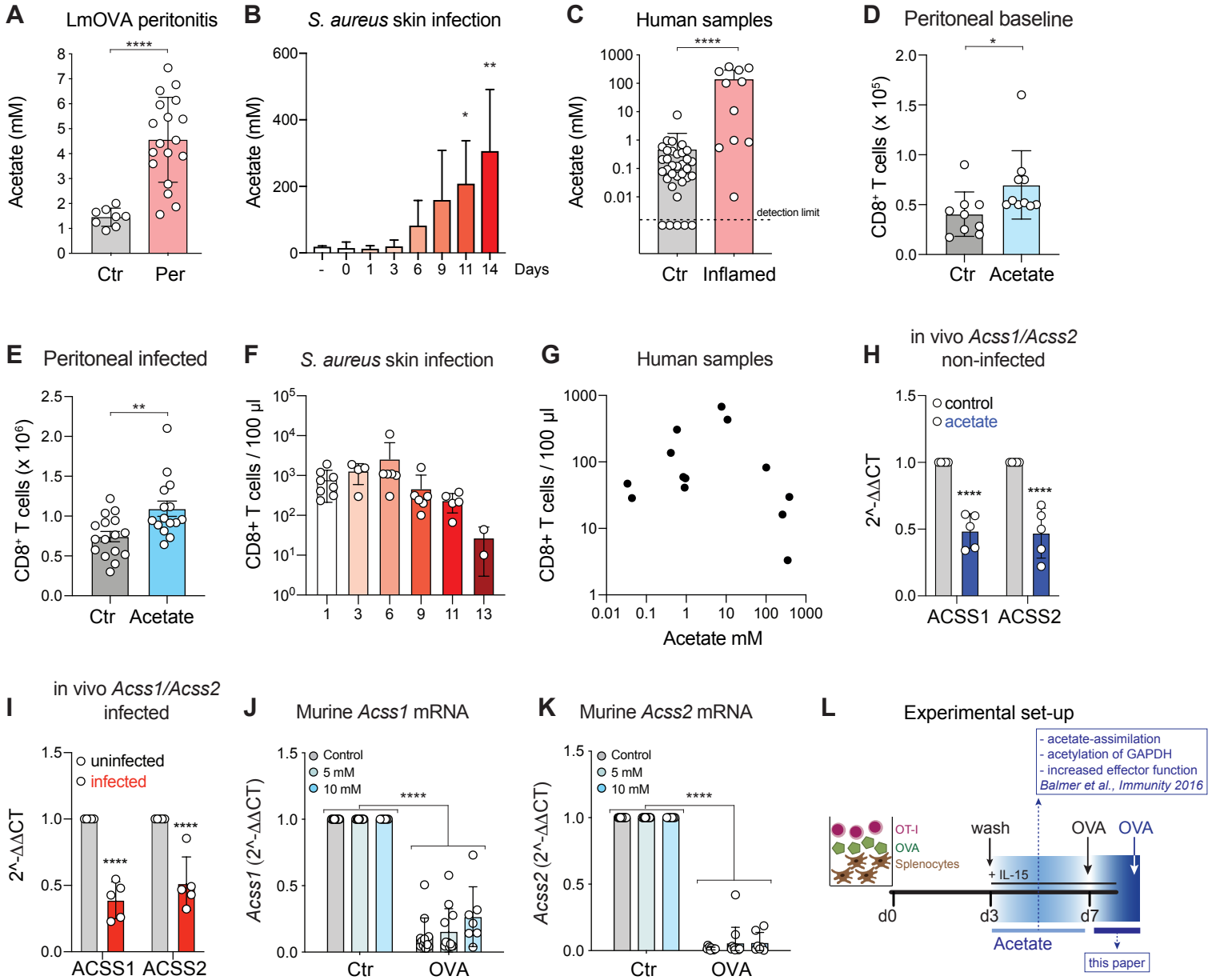
A
LmOVA peritonitis
Acetate (mM)
Ctr
Per
B
S. aureus skin infection
Acetate (mM)
Days
C
Human samples
Acetate (mM)
detection limit
Ctr
Inflamed
D
Peritoneal baseline
CD8+ T cells (x 10^5)
Ctr
Acetate
E
Peritoneal infected
CD8+ T cells (x 10^6)
Ctr
Acetate
F
S. aureus skin infection
CD8+ T cells / 100 µl
G
Human samples
CD8+ T cells / 100 µl
Acetate mM
H
in vivo Acss1/Acss2 non-infected
control
acetate
2^-ΔΔCT
ACSS1
ACSS2
I
in vivo Acss1/Acss2 infected
uninfected
infected
2^-ΔΔCT
ACSS1
ACSS2
J
Murine Acss1 mRNA
Control
5 mM
10 mM
Acss1 (2^-ΔΔCT)
Ctr
OVA
K
Murine Acss2 mRNA
Control
5 mM
10 mM
Acss2 (2^-ΔΔCT)
Ctr
OVA
L
Experimental set-up
- acetate-assimilation
- acetylation of GAPDH
- increased effector function
Balmer et al., Immunity 2016
OT-I
OVA
Splenocytes
wash
OVA
OVA
+ IL-15
d0
d3
d7
Acetate
this paper

Figure 2

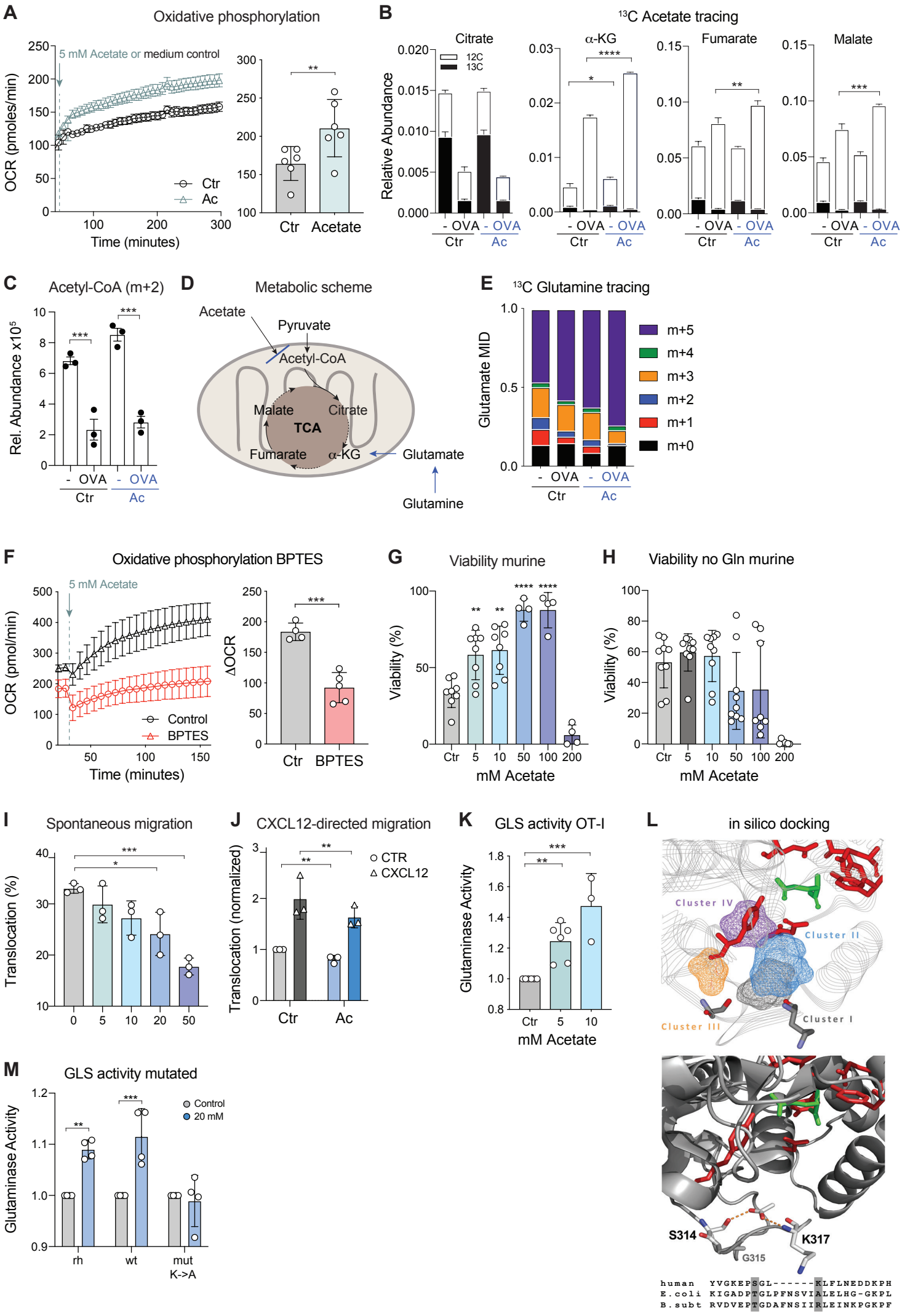

Balmer et al., Figure 2

Figure 3

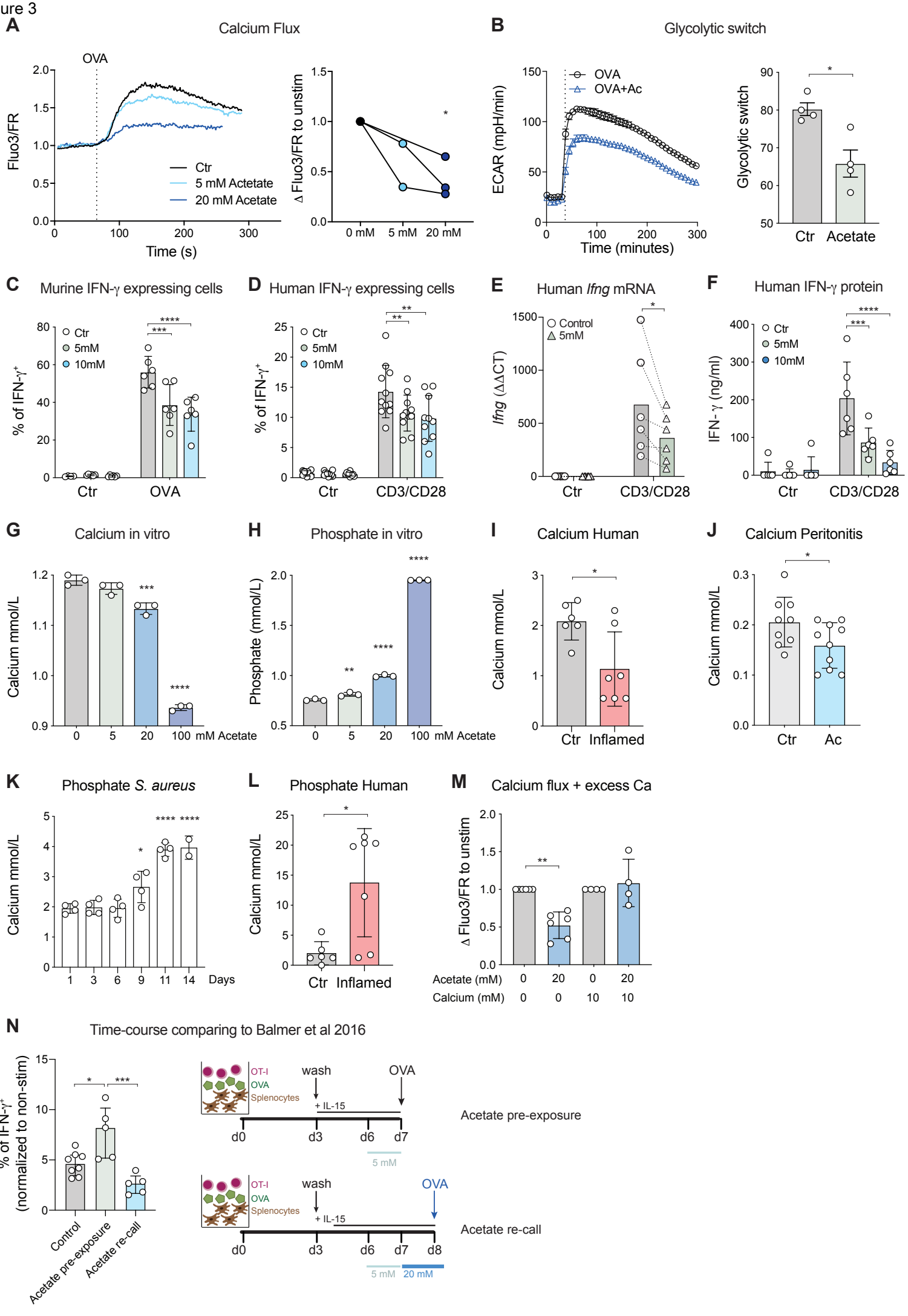

Balmer et al., Figure 3

Figure 4

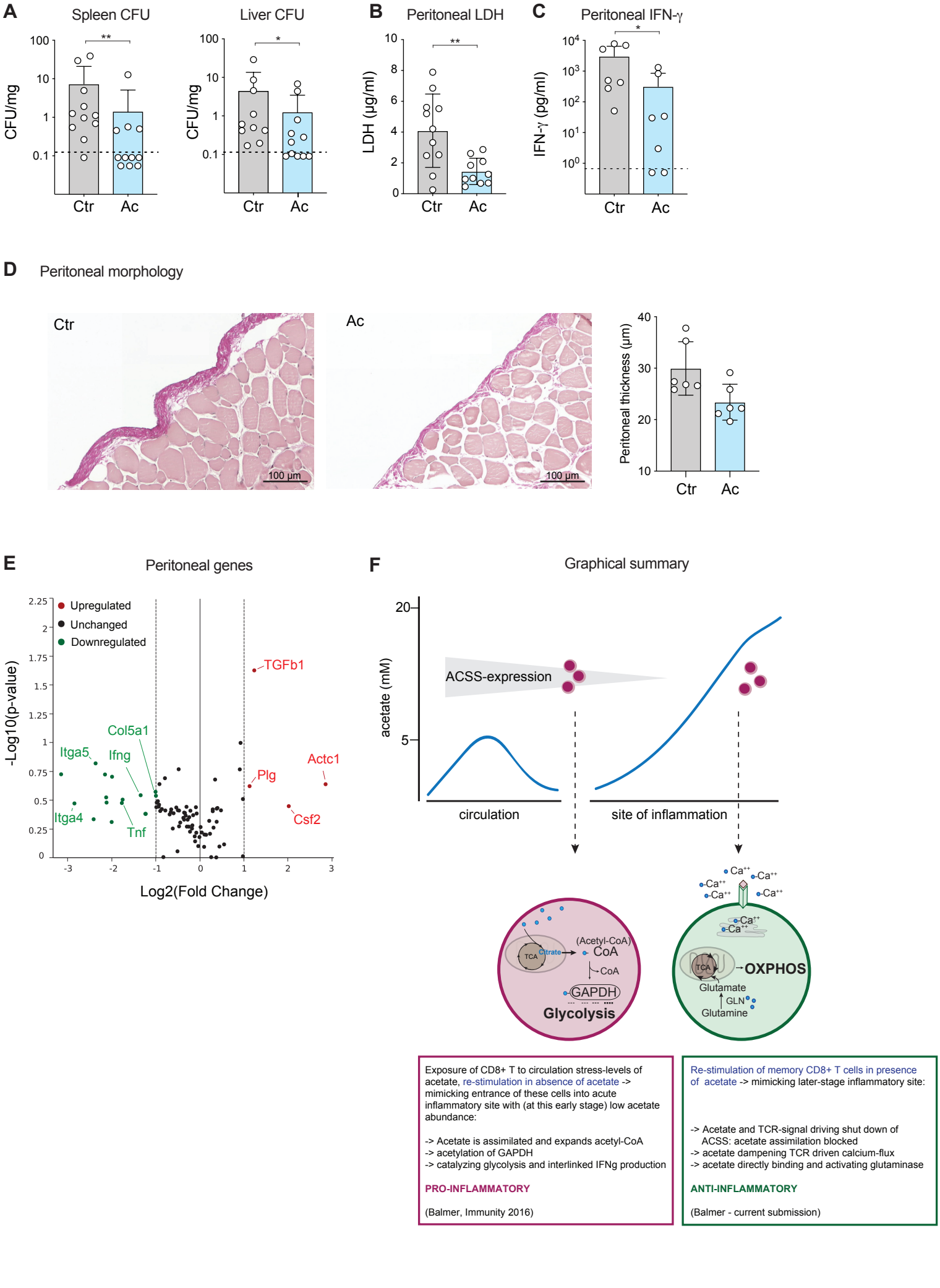

Exposure of CD8+ T to circulation stress-levels of acetate, re-stimulation in absence of acetate -> mimicking entrance of these cells into acute inflammatory site with (at this early stage) low acetate abundance:

-> Acetate is assimilated and expands acetyl-CoA
-> acetylation of GAPDH
-> catalyzing glycolysis and interlinked IFNg production

PRO-INFLAMMATORY

(Balmer, Immunity 2016)

Re-stimulation of memory CD8+ T cells in presence of acetate -> mimicking later-stage inflammatory site:

-> Acetate and TCR-signal driving shut down of ACSS: acetate assimilation blocked
-> acetate dampening TCR driven calcium-flux
-> acetate directly binding and activating glutaminase

ANTI-INFLAMMATORY

(Balmer - current submission)

KEY RESOURCES TABLE

REAGENT or RESOURCE	SOURCE	IDENTIFIER
Antibodies		
BUV395 rat anti-mouse CD44	BD	Cat# 740215
APC rat anti-mouse CD8	Biolegend	Cat# 100712
BV421 hamster anti-mouse KLRG1	Biolegend	Cat# 138413
PE rat anti-mouse CD62L	Biolegend	Cat# 104408
APC-Cy7 rat anti-mouse CD43	Biolegend	Cat# 121220
BV421 rat anti-mouse PDL1	Biolegend	Cat# 124315
PE-Cy5 rat anti-mouse CD127	eBioscience	Cat# 15-1271-82
PE rat anti-mouse CD25	Biolegend	Cat# 101904
BV510 hamster anti-mouse CD27	Biolegend	Cat# 124229
FITC rat anti-mouse CD3	BD	Cat# 555274
PE rat anti-mouse CD8	Biolegend	Cat# 100708
APC mouse anti-human CD62L	ImmunoTools	Cat# 21819626
Pacific Blue anti-CD45RA	Beckman Coulter	Cat# A86050
Bacterial and Virus Strains		
Listeria monocytogenes expressing chicken Ovalbumin (AA134–387)	Prof. Ed Palmer, University Basel, CH	
Biological Samples		
Human body fluids	University Hospital Basel	
Chemicals, Peptides, and Recombinant Proteins		
Liberase TL Research Grade	Roche	Cat#05 401 020 001
APC Annexin V	Immunotools	Cat#31490016
BPTES	Sigma Aldrich	Cat#SML0601
SB204990	Tocris	Cat#4962
Recombinant murine CXCL12	Peprotech	Cat#250-20A
Recombinant human glutaminase	R&D Systems	Cat#10115-GL-020
Glutaminase from E. coli	Megazyme	Cat#E-GLUTEC
Critical Commercial Assays		
Acetate fluorimetric assay kit	BioAssay Systems	Cat#EOAC-100
LDH Assay Kit	Abcam	Cat#ab102526
Glutaminase Microplate Assay Kit	Cohesion Biosciences	Cat#CAK1065
Experimental Models: Organisms/Strains		
Mouse: B6.129S6-Rag2tm1Fwa Tg(TcraTcrb)1100Mjb	Taconic	Model #2334
Mouse: C57BL/6	Charles River and Janvier	
Oligonucleotides		
ms ACSS1 (forward 5'-GTTTGGGACACTCCTTACCATAC-3' and reverse 5'-AGGCAGTTGACAGACACATTC-3')	Invitrogen	This paper
ms ACSS2 (forward 5'-GTGAAAGGATCTTGGATTCCAGT-3' and reverse 5'-CAGATGTTTGACCACAATGCAG-3')	Invitrogen	This paper
Gls: Mm01257297_m1	Thermo Fisher	Cat#4331182
Ifng: Mm01168134_m1	Thermo Fisher	Cat#4331182
ms 18S primers (forward 5'-GGGAGCCTGAGAAACGGC-3' and reverse 5'-GGGTCGGGAGTGGGTAATTT-3')	Microsynth	This paper
hs ACSS1 (forward 5'-CACAGGACAGACAACAAGGTC-3' and reverse 5'-CCTGGGTATGGAACGATGCC-3')	Invitrogen	This paper

hs ACSS2 (forward 5'-AAAGGAGCAACTACCAACATCTG-3' and reverse 5'-GCTGAACTGACACACTTGGAC-3')	Invitrogen	This paper
Human 18S	Applied Biosystems	Cat#4310893E
Recombinant DNA		
pGEX-4T-1-GLS2_WT (C-terminal GST)	Genscript	
pGEX-4T-1-GLS2_K253A (C-terminal GST)	Genscript	
Software and Algorithms		
FlowJo	BD	https://www.flowjo.com
GOLD Suite v5.7.0	The Cambridge Crystallographic Data Centre, Cambridge, UK	https://www.ch.cam.ac.uk/computing/software/gold-suite
PyMol v1.3	Schrödinger	https://pymol.org/2/
ImageJ		https://imagej.net/Welcome
GraphPad Prism		https://www.graphpad.com/scientific-software/prism/

Supplemental Text and Figures

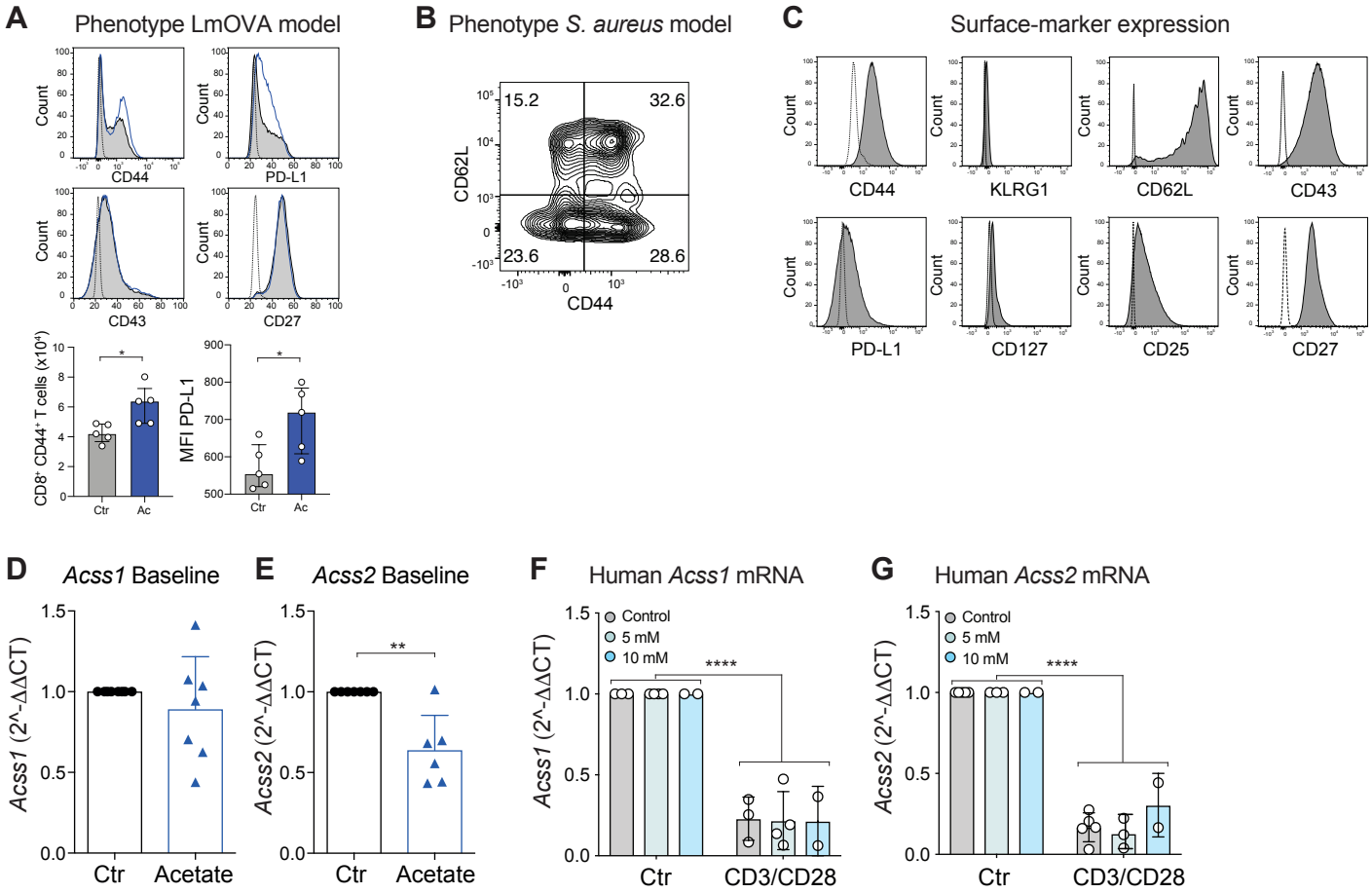

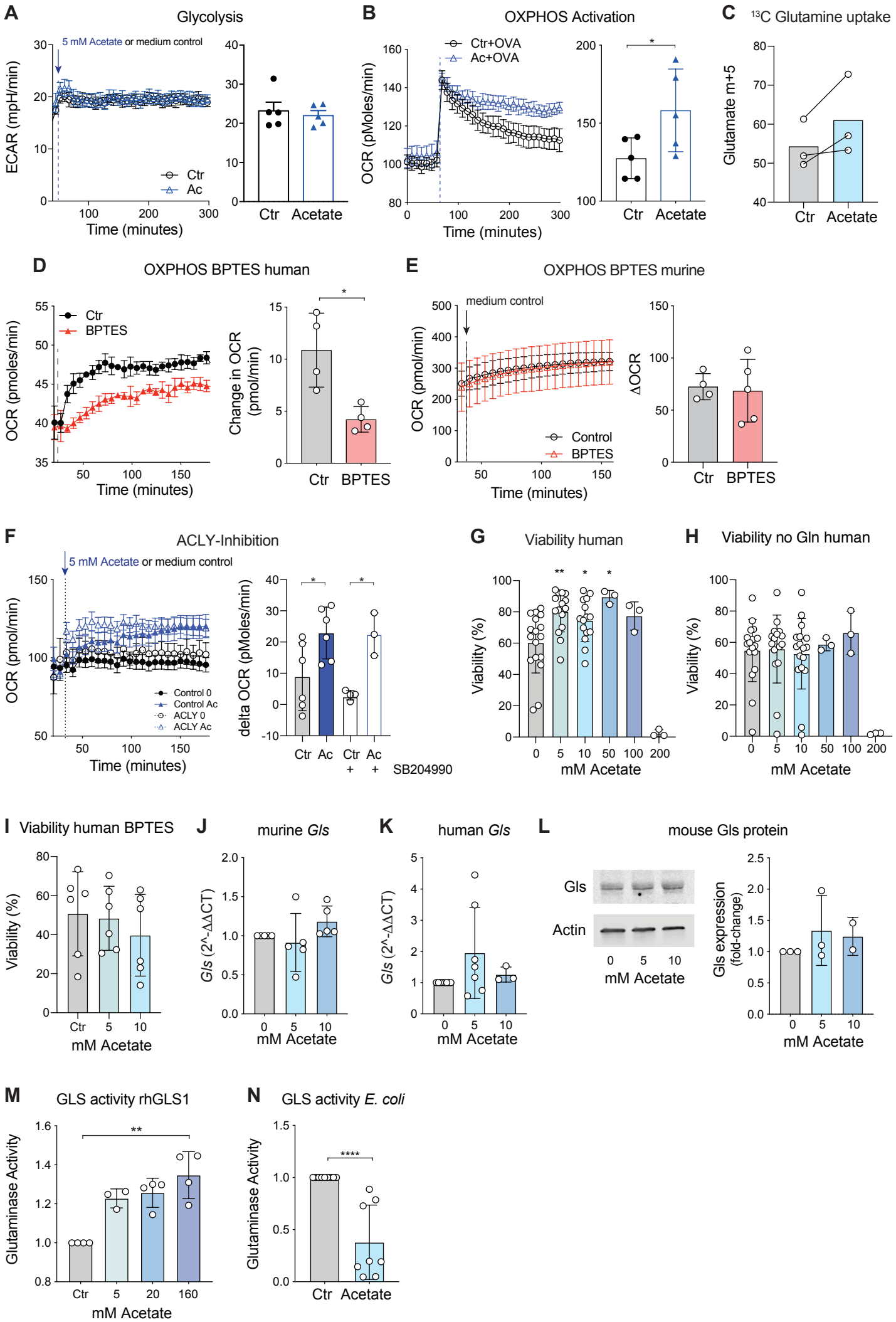

Balmer et al., Supplementary Figure 2

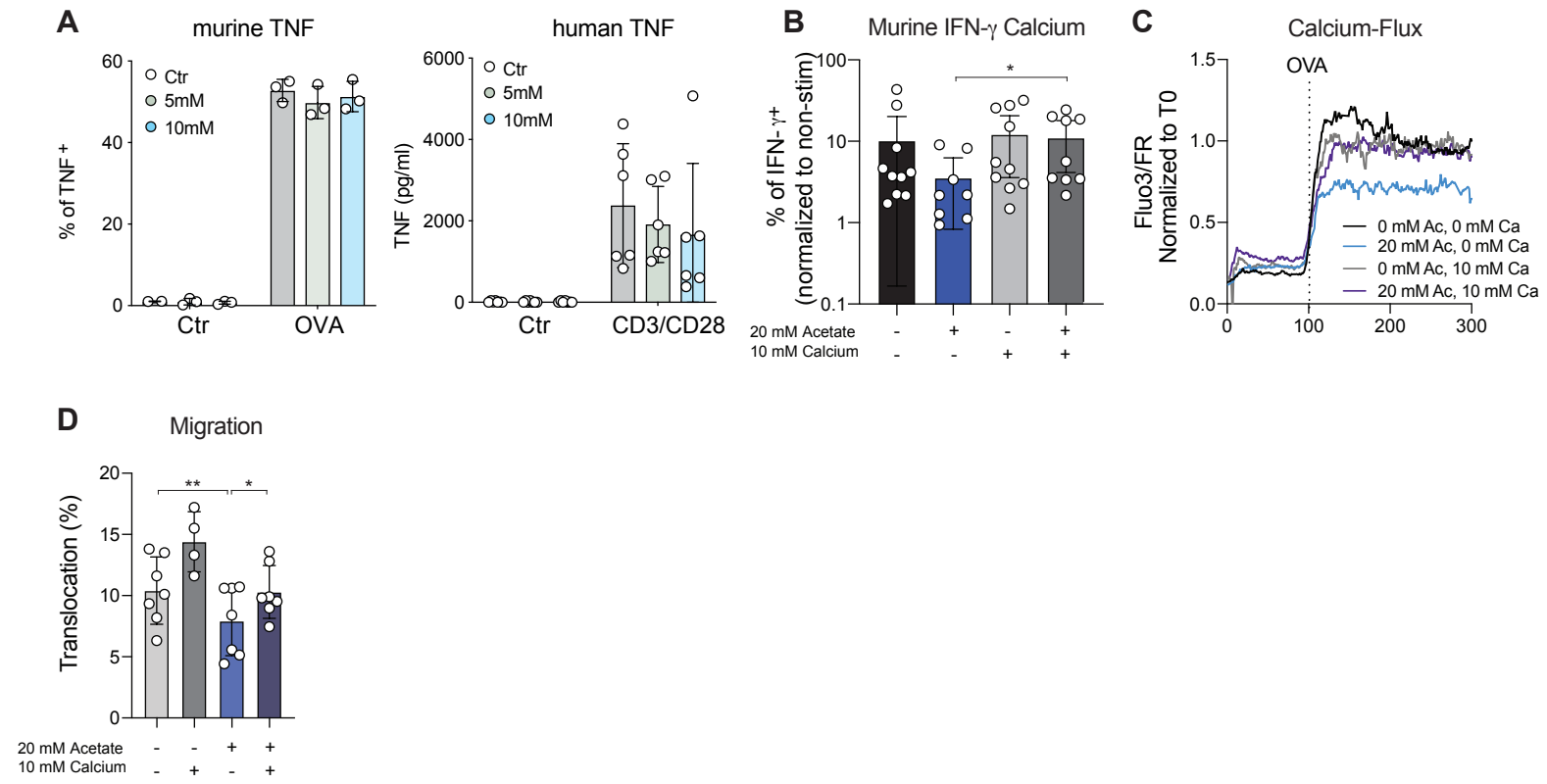
A
murine TNF
% of TNF+
Ctr
5mM
10mM
Ctr
OVA
human TNF
TNF (pg/ml)
Ctr
5mM
10mM
Ctr
CD3/CD28
B
Murine IFN-γ Calcium
% of IFN-γ+ (normalized to non-stim)
*
20 mM Acetate
10 mM Calcium
C
Calcium-Flux
OVA
Fluo3/FR Normalized to T0
0 mM Ac, 0 mM Ca
20 mM Ac, 0 mM Ca
0 mM Ac, 10 mM Ca
20 mM Ac, 10 mM Ca
D
Migration
Translocation (%)
**
*
20 mM Acetate
10 mM Calcium

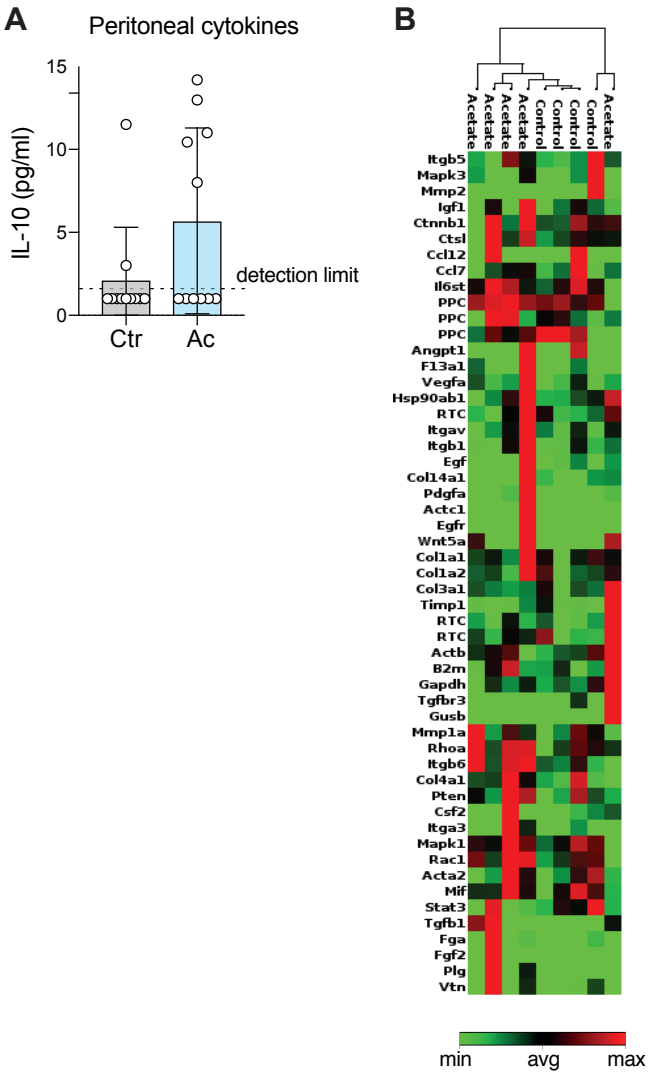
A
Peritoneal cytokines
IL-10 (pg/ml)
15
10
5
0
detection limit
Ctr
Ac
B
Acetate
Acetate
Acetate
Acetate
Control
Control
Control
Control
Itgb5
Mapk3
Mmp2
Igf1
Ctnnb1
Ctsl
Ccl12
Ccl7
Il6st
PPC
PPC
PPC
Angpt1
F13a1
Vegfa
Hsp90ab1
RTC
Itgav
Itgb1
Egf
Col14a1
Pdgfa
Actc1
Egfr
Wnt5a
Col1a1
Col1a2
Col3a1
Timp1
RTC
RTC
Actb
B2m
Gapdh
Tgfbr3
Gusb
Mmp1a
Rhoa
Itgb6
Col4a1
Pten
Csf2
Itga3
Mapk1
Rac1
Acta2
Mif
Stat3
Tgfb1
Fga
Fgf2
Plg
Vtn
min
avg
max

Supplementary Figure Legends

Supplementary Figure 1: *Effect of local acetate concentrations on memory CD8$^+$ T cell phenotype, related to figure 1.* **A**) Phenotype of MACS-purified CD8$^+$ T cells 24 h upon LmOVA-re-infection of LmOVA-immunized mice in presence (blue) or absence (gray) of 10 mM acetate as determined by flow cytometry. Shown are representative histograms and quantification of CD44$^+$ CD8$^+$ T cells and PD-L1 expression. The dashed lines indicate unstained controls. **B**) Phenotype of MACS-purified CD8$^+$ T cells of *S. aureus* tissue cage infection from day 6 of infection. Shown is a representative dot plot of n=5 mice. **C**) Surface marker expression of *in vitro* generated memory OT-I T cells. The dashed line indicates unstained controls. **D** and **E**) Baseline ACSS1 (**D**) and ACSS2 (**E**) expression in murine memory OT-I T cells after 4 h of incubation in control (black) or 5 mM acetate (blue) medium. **F** and **G**) Human effector memory CD8$^+$ T cells were re-stimulated with anti-CD3/CD28 for 4 h in presence/absence of the indicated acetate-concentrations or control medium. ACSS1 (**F**) and ACSS2 (**G**) expression was determined by RT-PCR.

Each dot represents one mouse or human. Lines indicate means, error bars are SD. T-test (**A**, **D** and **E**) and Two-way ANOVA (**F** and **G**) was used to compare the groups. * $P < 0.05$, ** $P < 0.01$, **** $P < 0.0001$

Supplementary Figure 2: *Increased glutaminolysis is important for viability and happens independently of glutaminase-expression, related to figure 2.* **A**) Memory OT-I T cells were analyzed by metabolic flux analysis upon injection of 5 mM acetate (blue) or medium control (black) at the beginning of the analysis (dashed line and arrow). Shown is a representative experiment of ECAR-values (left) and pooled data from 5 independent experiments (right) showing ECAR-values at 300 min. **B**) Memory OT-I T cells were re-stimulated with 10 µM OVA-peptide in seahorse in presence (blue) or absence (black) of 5 mM acetate (dashed line). Shown is a representative experiment of OCR-values (left) and pooled data from 5 independent experiments (right) showing OCR-values at 300 min. **C**) ^{13}C-glutamine tracing experiment of murine memory OT-I T cells cultured in presence or absence of 5 mM acetate for 4 h and analyzed upon 6 h of exposure to ^{13}C-glutamine. Shown is the m+5 abundance of ^{13}C-glutamate. **D**) Human effector memory CD8$^+$ T cells were pre-incubated in presence (red) or absence (black) of the glutaminase-inhibitor BPTES (50 µM) and subsequently analyzed by metabolic flux analysis upon injection of 5 mM acetate (dashed line) at the beginning of the analysis. Shown is a representative experiment of OCR-values (left) and pooled data from 4 independent experiments (right) calculating the net-increase of OCR from time 30 to 150 min. **E**) Memory OT-I T cells were pre-incubated in presence (red) or absence (black) of the glutaminase-inhibitor BPTES (50 µM) and subsequently analyzed by metabolic flux analysis. Shown is a representative experiment of OCR-values (left) and pooled data from 5 independent experiments (right) calculating the net-increase of OCR from time 30 to 150 min. **F**) Memory OT-I T cells were pre-incubated in presence (empty symbols) or absence (filled

symbols) of the ACLY-inhibitor SB204990 (30 µM) and subsequently analyzed by metabolic flux analysis upon injection of 5 mM acetate (blue) or medium control. Shown is a representative experiment of OCR-values (left) and pooled data from 3-5 independent experiments (right) calculating the net-increase of OCR from time 30 to 150 min. **G**-**I**) Viability of human effector memory $CD8^+$ T cells cultured *in vitro* for 5 days in presence (**G**) or absence (**H**) of glutamine in the culture medium, or in presence of BPTES (**I**), and the indicated acetate-concentrations. Viability was determined by flow cytometry using annexin V and PI staining. **J**-**L**) Murine (**J** and **L**) and human (**K**) memory $CD8^+$ T cells were incubated in the indicated acetate-concentrations for 4 h and glutaminase-expression analyzed by RT-PCR (**J** and **K**) and immunoblotting (**L**). Data in (**L**) are normalized to actin-expression and 0 mM acetate. **M**) Glutaminase activity of human recombinant glutaminase incubated for 15 min with the indicated acetate-concentrations. **N**) Glutaminase activity was determined in *E. coli* derived glutaminase, incubated in presence or absence of acetate for 1 h using a commercially available assay kit.

Each dot represents one mouse or human, lines indicate means, error bars are SD. T-test (**A**-**E**), Mann-Whitney test (**N**) or One-way ANOVA (**F**-**M**) were used to compare the groups. * $P < 0.05$, ** $P < 0.01$, **** $P < 0.0001$

Supplementary Figure 3: *Acetate suppresses calcium-availability to memory $CD8^+$ T cells and suppresses effector function, related to figure 3.* **A**) TNF production as assessed by intracellular cytokine staining in murine (left) or human (right) memory $CD8^+$ T cells 4 h after re-stimulation with 10 µM OVA-peptide or anti-CD3/CD28 antibodies in presence (blue) or absence (black) of indicated acetate-concentrations. **B**) IFN-γ production as assessed by intracellular cytokine staining in murine memory OT-I T cells 4 h after re-stimulation with 10 µM OVA-peptide in presence or absence of 20 mM acetate or 10 mM calcium. Data are normalized to the non-stimulated samples of each condition. **C**) Calcium-flux of the cells as treated in (**B**). **D**) Spontaneous migratory capacity of *in vitro* generated murine memory OT-I T cells analyzed in a transwell-assay in presence or absence of the indicated acetate and calcium-concentrations.

Each dot represents one mouse or human, lines indicate means, error bars are SD. One-way ANOVA (**B** and **D**) and Two-way ANOVA (**A**) was used to compare the groups. * $p < 0.05$, ** $P < 0.01$

Supplementary Figure 4: *Acetate shifts gene-expression towards an immunomodulatory phenotype, related to figure 4.* **A**) LmOVA-immunized mice were i.p. re-infected with 10^5 CFU LmOVA in presence (blue) or absence (black) of 10 mM acetate. IL-10 was measured in the peritoneal fluid by cytometric bead array. **B**) Heatmap of the PCR-Array from peritoneal tissue of the mice described in (**A**). Red indicates increased, green decreased gene-expression. Data was analyzed using the Qiagen RT^2 Profiler Analysis Software.

Each dot represents one mouse, lines indicate means, error bars are SD. Dashed lines indicate the detection limit. T-test was used to compare the groups (**A**).